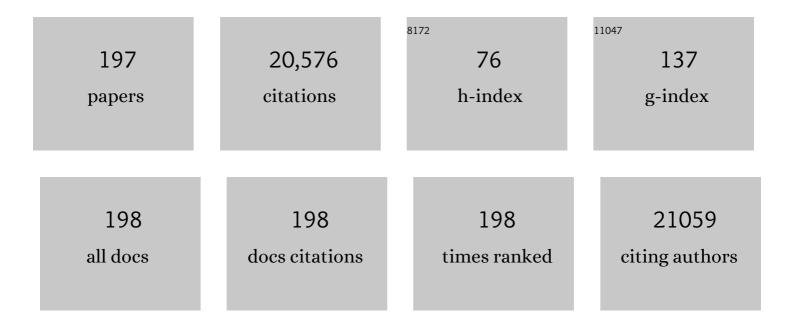
Yonghua Du

List of Publications by Year in descending order

Source: https://exaly.com/author-pdf/8452144/publications.pdf Version: 2024-02-01



| # | Article | IF | CITATIONS |
|----|---|------|-----------|
| 1 | Metal″on Oligomerization Inside Electrified Carbon Micropores and its Effect on Capacitive Charge Storage. Advanced Materials, 2022, 34, e2107439. | 11.1 | 24 |
| 2 | An ultrathin solid-state electrolyte film coated on LiNi0.8Co0.1Mn0.1O2 electrode surface for enhanced performance of lithium-ion batteries. Energy Storage Materials, 2022, 45, 1165-1174. | 9.5 | 43 |
| 3 | CO2-assisted ethane aromatization over zinc and phosphorous modified ZSM-5 catalysts. Applied Catalysis B: Environmental, 2022, 304, 120956. | 10.8 | 21 |
| 4 | Intercalationâ€Activated Layered MoO ₃ Nanobelts as Biodegradable Nanozymes for Tumorâ€Specific Photoâ€Enhanced Catalytic Therapy. Angewandte Chemie - International Edition, 2022, 61, . | 7.2 | 109 |
| 5 | Intercalationâ€Activated Layered MoO ₃ Nanobelts as Biodegradable Nanozymes for Tumorâ€Specific Photoâ€Enhanced Catalytic Therapy. Angewandte Chemie, 2022, 134, . | 1.6 | 16 |
| 6 | CO2 hydrogenation to methanol on tungsten-doped Cu/CeO2 catalysts. Applied Catalysis B: Environmental, 2022, 306, 121098. | 10.8 | 50 |
| 7 | Amorphizing noble metal chalcogenide catalysts at the single-layer limit towards hydrogen production. Nature Catalysis, 2022, 5, 212-221. | 16.1 | 113 |
| 8 | Hybrid MoS _{2+<i>x</i>} Nanosheet/Nanocarbon Heterostructures for Lithium-Ion Batteries. ACS Applied Nano Materials, 2022, 5, 5103-5118. | 2.4 | 7 |
| 9 | Atomically Precise Single Metal Oxide Cluster Catalyst with Oxygen ontrolled Activity. Advanced Functional Materials, 2022, 32, . | 7.8 | 13 |
| 10 | First demonstration of tuning between the Kitaev and Ising limits in a honeycomb lattice. Science Advances, 2022, 8, eabl5671. | 4.7 | 6 |
| 11 | Saltâ€Assisted 2Hâ€toâ€1T′ Phase Transformation of Transition Metal Dichalcogenides. Advanced Materials, 2022, 34, e2201194. | 11.1 | 19 |
| 12 | Fluorine-tuned single-atom catalysts with dense surface Ni-N4 sites on ultrathin carbon nanosheets for efficient CO2 electroreduction. Applied Catalysis B: Environmental, 2021, 283, 119591. | 10.8 | 116 |
| 13 | Sandwich structure stabilized atomic Fe catalyst for highly efficient Fenton-like reaction at all pH values. Applied Catalysis B: Environmental, 2021, 282, 119551. | 10.8 | 93 |
| 14 | Molecular engineered palladium single atom catalysts with an M-C ₁ N ₃ subunit for Suzuki coupling. Journal of Materials Chemistry A, 2021, 9, 11427-11432. | 5.2 | 18 |
| 15 | Activating Layered Metal Oxide Nanomaterials via Structural Engineering as Biodegradable Nanoagents for Photothermal Cancer Therapy. Small, 2021, 17, e2007486. | 5.2 | 94 |
| 16 | Evoking ordered vacancies in metallic nanostructures toward a vacated Barlow packing for high-performance hydrogen evolution. Science Advances, 2021, 7, . | 4.7 | 64 |
| 17 | Reversible hydrogen control of antiferromagnetic anisotropy in α-Fe2O3. Nature Communications, 2021, 12, 1668. | 5.8 | 30 |
| 18 | Highly Selective Acetylene Semihydrogenation Catalyst with an Operation Window Exceeding 150 °C. ACS Catalysis, 2021, 11, 6073-6080. | 5.5 | 33 |

Үолдниа Du

| # | Article | IF | CITATIONS |
|----|--|------|-----------|
| 19 | Coordinatively and Spatially Coconfining High-Loading Atomic Sb in Sulfur-Rich 2D Carbon Matrix for Fast K ⁺ Diffusion and Storage. , 2021, 3, 790-798. | | 10 |
| 20 | Tuning of lattice oxygen reactivity and scaling relation to construct better oxygen evolution electrocatalyst. Nature Communications, 2021, 12, 3992. | 5.8 | 151 |
| 21 | Understanding the Roles of the Electrode/Electrolyte Interface for Enabling Stable Liâ^¥Sulfurized Polyacrylonitrile Batteries. ACS Applied Materials & Interfaces, 2021, 13, 31733-31740. | 4.0 | 25 |
| 22 | Zeroâ€Valent Palladium Singleâ€Atoms Catalysts Confined in Black Phosphorus for Efficient Semiâ€Hydrogenation. Advanced Materials, 2021, 33, e2008471. | 11.1 | 55 |
| 23 | Surface coupling of methyl radicals for efficient low-temperature oxidative coupling of methane. Chinese Journal of Catalysis, 2021, 42, 1117-1125. | 6.9 | 39 |
| 24 | Self-assembled iron-containing mordenite monolith for carbon dioxide sieving. Science, 2021, 373, 315-320. | 6.0 | 179 |
| 25 | Grafting nanometer metal/oxide interface towards enhanced low-temperature acetylene semi-hydrogenation. Nature Communications, 2021, 12, 5770. | 5.8 | 43 |
| 26 | Promoting the Oxygen Evolution Activity of Perovskite Nickelates through Phase Engineering. ACS Applied Materials & Interfaces, 2021, 13, 58566-58575. | 4.0 | 30 |
| 27 | Direct methanation with supported MoS2 nano-flakes: Relationship between structure and activity. Catalysis Today, 2020, 342, 21-31. | 2.2 | 13 |
| 28 | Bismuth ion battery – A new member in trivalent battery technology. Energy Storage Materials, 2020, 25, 100-104. | 9.5 | 3 |
| 29 | Strain stabilized nickel hydroxide nanoribbons for efficient water splitting. Energy and Environmental Science, 2020, 13, 229-237. | 15.6 | 78 |
| 30 | γ-Al2O3 sheet-stabilized isolate Co2+ for catalytic propane dehydrogenation. Journal of Catalysis, 2020, 381, 482-492. | 3.1 | 98 |
| 31 | Phase-Selective Epitaxial Growth of Heterophase Nanostructures on Unconventional 2H-Pd Nanoparticles. Journal of the American Chemical Society, 2020, 142, 18971-18980. | 6.6 | 111 |
| 32 | The interplay between the suprafacial and intrafacial mechanisms for complete methane oxidation on substituted LaCoO3 perovskite oxides. Journal of Catalysis, 2020, 390, 1-11. | 3.1 | 32 |
| 33 | Mesoporous 3D/2D NiCoP/g-C ₃ N ₄ Heterostructure with Dual Co–N and Ni–N Bonding States for Boosting Photocatalytic H ₂ Production Activity and Stability. ACS Sustainable Chemistry and Engineering, 2020, 8, 12934-12943. | 3.2 | 45 |
| 34 | Multimodal, Multidimensional, and Multiscale X-ray Imaging at the National Synchrotron Light Source II. Synchrotron Radiation News, 2020, 33, 29-36. | 0.2 | 5 |
| 35 | Atomically-precise dopant-controlled single cluster catalysis for electrochemical nitrogen reduction. Nature Communications, 2020, 11, 4389. | 5.8 | 110 |
| 36 | Materializing efficient methanol oxidation via electron delocalization in nickel hydroxide nanoribbon. Nature Communications, 2020, 11, 4647. | 5.8 | 117 |

| # | Article | IF | CITATIONS |
|----|---|------|-----------|
| 37 | Covalency competition dominates the water oxidation structure–activity relationship on spinel oxides. Nature Catalysis, 2020, 3, 554-563. | 16.1 | 284 |
| 38 | Rational Design and Synthesis of Hierarchical Porous Mn–N–C Nanoparticles with Atomically Dispersed MnN <i>_x</i> Moieties for Highly Efficient Oxygen Reduction Reaction. ACS Sustainable Chemistry and Engineering, 2020, 8, 9367-9376. | 3.2 | 43 |
| 39 | 2D Boron Imidazolate Framework Nanosheets with Electrocatalytic Applications for Oxygen Evolution and Carbon Dioxide Reduction Reaction. Small, 2020, 16, e1907669. | 5.2 | 20 |
| 40 | Constructing an Adaptive Heterojunction as a Highly Active Catalyst for the Oxygen Evolution Reaction. Advanced Materials, 2020, 32, e2001292. | 11.1 | 122 |
| 41 | Spatially separating redox centers on 2D carbon nitride with cobalt single atom for photocatalytic H ₂ O ₂ production. Proceedings of the National Academy of Sciences of the United States of America, 2020, 117, 6376-6382. | 3.3 | 245 |
| 42 | Engineering Local and Global Structures of Single Co Atoms for a Superior Oxygen Reduction Reaction. ACS Catalysis, 2020, 10, 5862-5870. | 5.5 | 126 |
| 43 | Dielectric Polarization in Inverse Spinelâ€Structured Mg ₂ TiO ₄ Coating to Suppress Oxygen Evolution of Liâ€Rich Cathode Materials. Advanced Materials, 2020, 32, e2000496. | 11.1 | 134 |
| 44 | Metal Atomâ€Đoped Co ₃ O ₄ Hierarchical Nanoplates for Electrocatalytic Oxygen Evolution. Advanced Materials, 2020, 32, e2002235. | 11.1 | 332 |
| 45 | Probing the Oxidation/Reduction Dynamics of Fresh and P-, Na-, and K-Contaminated Pt/Pd/Al ₂ O ₃ Diesel Oxidation Catalysts by STEM, TPR, and in Situ XANES. Journal of Physical Chemistry C, 2020, 124, 2945-2952. | 1.5 | 10 |
| 46 | Ligandâ€Exchangeâ€Induced Amorphization of Pd Nanomaterials for Highly Efficient Electrocatalytic Hydrogen Evolution Reaction. Advanced Materials, 2020, 32, e1902964. | 11.1 | 164 |
| 47 | Enhanced Electrocatalytic Hydrogen Evolution Activity in Single-Atom Pt-Decorated VS ₂ Nanosheets. ACS Nano, 2020, 14, 5600-5608. | 7.3 | 135 |
| 48 | Antiferromagnetic Inverse Spinel Oxide LiCoVO ₄ with Spinâ€Polarized Channels for Water Oxidation. Advanced Materials, 2020, 32, e1907976. | 11.1 | 106 |
| 49 | Introduction of the Sirepo-Bluesky interface and its application to the optimization problems. , 2020, , . | | 2 |
| 50 | Defect-Rich, Candied Haws-Shaped AuPtNi Alloy Nanostructures for Highly Efficient Electrocatalysis. CCS Chemistry, 2020, 2, 24-30. | 4.6 | 23 |
| 51 | Unraveling the Formation of Amorphous MoS ₂ Nanograins during the Electrochemical Delithiation Process. Advanced Functional Materials, 2019, 29, 1904843. | 7.8 | 38 |
| 52 | Iron-facilitated dynamic active-site generation on spinel CoAl2O4 with self-termination of surface reconstruction for water oxidation. Nature Catalysis, 2019, 2, 763-772. | 16.1 | 678 |
| 53 | Linkage Effect in the Heterogenization of Cobalt Complexes by Doped Graphene for Electrocatalytic CO ₂ Reduction. Angewandte Chemie - International Edition, 2019, 58, 13532-13539. | 7.2 | 143 |
| 54 | Linkage Effect in the Heterogenization of Cobalt Complexes by Doped Graphene for Electrocatalytic CO ₂ Reduction. Angewandte Chemie, 2019, 131, 13666-13673. | 1.6 | 24 |

| # | Article | IF | CITATIONS |
|----|---|------|-----------|
| 55 | A Grapheneâ€Supported Singleâ€Atom FeN ₅ Catalytic Site for Efficient Electrochemical CO ₂ Reduction. Angewandte Chemie, 2019, 131, 15013-15018. | 1.6 | 107 |
| 56 | A Grapheneâ€Supported Singleâ€Atom FeN ₅ Catalytic Site for Efficient Electrochemical CO ₂ Reduction. Angewandte Chemie - International Edition, 2019, 58, 14871-14876. | 7.2 | 410 |
| 57 | Electronic and Geometric Structures of Rechargeable Lithium Manganese Sulfate Li ₂ Mn(SO ₄) ₂ Cathode. ACS Omega, 2019, 4, 11338-11345. | 1.6 | 2 |
| 58 | αâ€Ni(OH) ₂ Originated from Electroâ€Oxidation of NiSe ₂ Supported by Carbon Nanoarray on Carbon Cloth for Efficient Water Oxidation. Small, 2019, 15, e1902222. | 5.2 | 18 |
| 59 | Optimizing interfacial electronic coupling with metal oxide to activate inert polyaniline for superior electrocatalytic hydrogen generation. , 2019, 1, 77-84. | | 50 |
| 60 | Highly Efficient Multifunctional Co–N–C Electrocatalysts with Synergistic Effects of Co–N Moieties and Co Metallic Nanoparticles Encapsulated in a N-Doped Carbon Matrix for Water-Splitting and Oxygen Redox Reactions. ACS Applied Materials & Interfaces, 2019, 11, 39809-39819. | 4.0 | 80 |
| 61 | Confinement-Induced Giant Spin–Orbit-Coupled Magnetic Moment of Co Nanoclusters in TiO ₂ Films. ACS Applied Materials & Interfaces, 2019, 11, 43781-43788. | 4.0 | 8 |
| 62 | Interfacial Latticeâ€Strainâ€Driven Generation of Oxygen Vacancies in an Aerobicâ€Annealed TiO ₂ (B) Electrode. Advanced Materials, 2019, 31, e1906156. | 11.1 | 53 |
| 63 | Lowering Charge Transfer Barrier of LiMn ₂ O ₄ via Nickel Surface Doping To Enhance Li ⁺ Intercalation Kinetics at Subzero Temperatures. Journal of the American Chemical Society, 2019, 141, 14038-14042. | 6.6 | 125 |
| 64 | Copper Single Atoms Anchored in Porous Nitrogen-Doped Carbon as Efficient pH-Universal Catalysts for the Nitrogen Reduction Reaction. ACS Catalysis, 2019, 9, 10166-10173. | 5.5 | 284 |
| 65 | Boosting Electrochemical CO ₂ Reduction on Metal–Organic Frameworks via Ligand Doping. Angewandte Chemie - International Edition, 2019, 58, 4041-4045. | 7.2 | 199 |
| 66 | Mastering Surface Reconstruction of Metastable Spinel Oxides for Better Water Oxidation. Advanced Materials, 2019, 31, e1807898. | 11.1 | 215 |
| 67 | Highly dispersed nickel catalysts <i>via</i> a facile pyrolysis generated protective carbon layer. Chemical Communications, 2019, 55, 6074-6077. | 2.2 | 29 |
| 68 | Highly active N,S co-doped hierarchical porous carbon nanospheres from green and template-free method for super capacitors and oxygen reduction reaction. Electrochimica Acta, 2019, 318, 272-280. | 2.6 | 60 |
| 69 | Interaction of Copper Phthalocyanine with Nitrogen Dioxide and Ammonia Investigation Using X-ray Absorption Spectroscopy and Chemiresistive Gas Measurements. ACS Omega, 2019, 4, 10388-10395. | 1.6 | 27 |
| 70 | Na ₃ V ₂ (PO ₄) ₃ as the Sole Solid Energy Storage Material for Redox Flow Sodiumâ€ion Battery. Advanced Energy Materials, 2019, 9, 1901188. | 10.2 | 38 |
| 71 | Origin of electronic structure dependent activity of spinel ZnNixCo2-xO4 oxides for complete methane oxidation. Applied Catalysis B: Environmental, 2019, 256, 117844. | 10.8 | 35 |
| 72 | Stimulated Electrocatalytic Hydrogen Evolution Activity of MOFâ€Derived MoS ₂ Basal Domains via Charge Injection through Surface Functionalization and Heteroatom Doping. Advanced Science, 2019, 6, 1900140. | 5.6 | 73 |

Үолдниа Du

| # | Article | IF | CITATIONS |
|----|---|------|-----------|
| 73 | Single-Atom Coated Separator for Robust Lithium–Sulfur Batteries. ACS Applied Materials & Interfaces, 2019, 11, 25147-25154. | 4.0 | 152 |
| 74 | Guided Assembly of Microporous/Mesoporous Manganese Phosphates by Bifunctional Organophosphonic Acid Etching and Templating. Advanced Materials, 2019, 31, e1901124. | 11.1 | 15 |
| 75 | Aurophilic Interactions in the Selfâ€Assembly of Gold Nanoclusters into Nanoribbons with Enhanced Luminescence. Angewandte Chemie, 2019, 131, 8223-8228. | 1.6 | 29 |
| 76 | Nitrogen-Doped Cobalt Phosphide for Enhanced Hydrogen Evolution Activity. ACS Applied Materials & Interfaces, 2019, 11, 17359-17367. | 4.0 | 40 |
| 77 | Local Ca-structure variation and microstructural characteristics on one-part activated slag system with various activators. Cement and Concrete Composites, 2019, 102, 1-13. | 4.6 | 11 |
| 78 | Shifting Oxygen Charge Towards Octahedral Metal: A Way to Promote Water Oxidation on Cobalt Spinel Oxides. Angewandte Chemie, 2019, 131, 6103-6108. | 1.6 | 69 |
| 79 | Molecular-level design of Fe-N-C catalysts derived from Fe-dual pyridine coordination complexes for highly efficient oxygen reduction. Journal of Catalysis, 2019, 372, 245-257. | 3.1 | 56 |
| 80 | Chemical and structural origin of lattice oxygen oxidation in Co–Zn oxyhydroxide oxygen evolution electrocatalysts. Nature Energy, 2019, 4, 329-338. | 19.8 | 977 |
| 81 | Hybrid MOF-808-Tb nanospheres for highly sensitive and selective detection of acetone vapor and Fe ³⁺ in aqueous solution. Chemical Communications, 2019, 55, 4727-4730. | 2.2 | 61 |
| 82 | Shifting Oxygen Charge Towards Octahedral Metal: A Way to Promote Water Oxidation on Cobalt Spinel Oxides. Angewandte Chemie - International Edition, 2019, 58, 6042-6047. | 7.2 | 226 |
| 83 | Aurophilic Interactions in the Selfâ€Assembly of Gold Nanoclusters into Nanoribbons with Enhanced Luminescence. Angewandte Chemie - International Edition, 2019, 58, 8139-8144. | 7.2 | 185 |
| 84 | Exceptionally active iridium evolved from a pseudo-cubic perovskite for oxygen evolution in acid. Nature Communications, 2019, 10, 572. | 5.8 | 254 |
| 85 | A Flexible Microwave Shield with Tunable Frequencyâ€Transmission and Electromagnetic Compatibility. Advanced Functional Materials, 2019, 29, 1900163. | 7.8 | 299 |
| 86 | Defect Engineering of Oxygenâ€Đeficient Manganese Oxide to Achieve Highâ€Performing Aqueous Zinc Ion Battery. Advanced Energy Materials, 2019, 9, 1803815. | 10.2 | 504 |
| 87 | Redox Targeting-Based Vanadium Redox-Flow Battery. ACS Energy Letters, 2019, 4, 3028-3035. | 8.8 | 63 |
| 88 | Expedient synthesis of <i>E</i> -hydrazone esters and 1 <i>H</i> -indazole scaffolds through heterogeneous single-atom platinum catalysis. Science Advances, 2019, 5, eaay1537. | 4.7 | 31 |
| 89 | Tuning the Electronic Structure of NiO via Li Doping for the Fast Oxygen Evolution Reaction. Chemistry of Materials, 2019, 31, 419-428. | 3.2 | 78 |
| 90 | High-Magnetization Tetragonal Ferrite-Based Films Induced by Carbon and Oxygen Vacancy Pairs. ACS Applied Materials & Interfaces, 2019, 11, 1049-1056. | 4.0 | 5 |

| # | Article | IF | CITATIONS |
|-----|---|------|-----------|
| 91 | Promoted Glycerol Oxidation Reaction in an Interfaceâ€Confined Hierarchically Structured Catalyst. Advanced Materials, 2019, 31, e1804763. | 11.1 | 40 |
| 92 | Approaching the Lithiation Limit of MoS ₂ While Maintaining Its Layered Crystalline Structure to Improve Lithium Storage. Angewandte Chemie - International Edition, 2019, 58, 3521-3526. | 7.2 | 62 |
| 93 | 2D carbide nanomeshes and their assembling into 3D microflowers for efficient water splitting. Applied Catalysis B: Environmental, 2019, 243, 678-685. | 10.8 | 116 |
| 94 | In Situ Electrochemical Conversion of an Ultrathin Tannin Nickel Iron Complex Film as an Efficient Oxygen Evolution Reaction Electrocatalyst. Angewandte Chemie - International Edition, 2019, 58, 3769-3773. | 7.2 | 188 |
| 95 | Understanding the Nature of Ammonia Treatment to Synthesize Oxygen Vacancy-Enriched Transition Metal Oxides. CheM, 2019, 5, 376-389. | 5.8 | 171 |
| 96 | In situ depth-resolved synchrotron radiation X-ray spectroscopy study of radiation-induced Au deposition. Journal of Synchrotron Radiation, 2019, 26, 1940-1944. | 1.0 | 1 |
| 97 | Annealing effect on the ferromagnetism of MoS2 nanoparticles. Journal of Alloys and Compounds, 2018, 746, 399-404. | 2.8 | 27 |
| 98 | Transitionâ€Metalâ€Doped αâ€MnO ₂ Nanorods as Bifunctional Catalysts for Efficient Oxygen Reduction and Evolution Reactions. ChemistrySelect, 2018, 3, 2613-2622. | 0.7 | 54 |
| 99 | Silica–Ceria sandwiched Ni core–shell catalyst for low temperature dry reforming of biogas: Coke resistance and mechanistic insights. Applied Catalysis B: Environmental, 2018, 230, 220-236. | 10.8 | 370 |
| 100 | Operando Investigation of Mn ₃ O _{4+δ} Co-catalyst on Fe ₂ O ₃ Photoanode: Manganese-Valency-Determined Enhancement at Varied Potentials. ACS Applied Energy Materials, 2018, 1, 814-821. | 2.5 | 21 |
| 101 | Superexchange Effects on Oxygen Reduction Activity of Edgeâ€Sharing [Co <i>_x</i> Mn _{1â^'} <i>_x</i> O ₆] Octahedra in Spinel Oxide. Advanced Materials, 2018, 30, 1705407. | 11.1 | 142 |
| 102 | Enhanced Catalysis of the Electrochemical Oxygen Evolution Reaction by Iron(III) Ions Adsorbed on Amorphous Cobalt Oxide. ACS Catalysis, 2018, 8, 807-814. | 5.5 | 163 |
| 103 | Mo-Terminated Edge Reconstructions in Nanoporous Molybdenum Disulfide Film. Nano Letters, 2018, 18, 482-490. | 4.5 | 105 |
| 104 | Preparation of Highâ€Percentage 1Tâ€Phase Transition Metal Dichalcogenide Nanodots for Electrochemical Hydrogen Evolution. Advanced Materials, 2018, 30, 1705509. | 11.1 | 341 |
| 105 | Cobalt Boron Imidazolate Framework Derived Cobalt Nanoparticles Encapsulated in B/N Codoped Nanocarbon as Efficient Bifunctional Electrocatalysts for Overall Water Splitting. Advanced Functional Materials, 2018, 28, 1801136. | 7.8 | 155 |
| 106 | Heteroatomic Znâ€MWW Zeolite Developed for Catalytic Dehydrogenation Reactions: A Combined Experimental and DFT Study. ChemCatChem, 2018, 10, 3078-3085. | 1.8 | 8 |
| 107 | High phase-purity 1T′-MoS2- and 1T′-MoSe2-layered crystals. Nature Chemistry, 2018, 10, 638-643. | 6.6 | 757 |
| 108 | Spinel Manganese Ferrites for Oxygen Electrocatalysis: Effect of Mn Valency and Occupation Site. Electrocatalysis, 2018, 9, 287-292. | 1.5 | 38 |

Уомдниа Du

| # | Article | IF | CITATIONS |
|-----|--|------|-----------|
| 109 | A Highly Efficient Oxygen Evolution Catalyst Consisting of Interconnected Nickel–Iron‣ayered Double Hydroxide and Carbon Nanodomains. Advanced Materials, 2018, 30, 1705106. | 11.1 | 209 |
| 110 | Revealing the Dominant Chemistry for Oxygen Reduction Reaction on Small Oxide Nanoparticles. ACS Catalysis, 2018, 8, 673-677. | 5.5 | 58 |
| 111 | Activation of the MoSe ₂ basal plane and Se-edge by B doping for enhanced hydrogen evolution. Journal of Materials Chemistry A, 2018, 6, 510-515. | 5.2 | 110 |
| 112 | Elucidation of thermally induced internal porosity in zinc oxide nanorods. Nano Research, 2018, 11, 2412-2423. | 5.8 | 10 |
| 113 | Mussel-inspired facile synthesis of Fe/Co-polydopamine complex nanospheres: complexation mechanism and application of the carbonized hybrid nanospheres as an efficient bifunctional electrocatalyst. New Journal of Chemistry, 2018, 42, 19494-19504. | 1.4 | 6 |
| 114 | Câ^'O Hydrogenolysis of Tetrahydrofurfuryl Alcohol to 1,5â€Pentanediol Over Biâ€functional Nickelâ€ī ungsten Catalysts. ChemCatChem, 2018, 10, 4652-4664. | 1.8 | 28 |
| 115 | Vanadium-embedded mesoporous carbon microspheres as effective catalysts for selective aerobic oxidation of 5-hydroxymethyl-2-furfural into 2, 5-diformylfuran. Applied Catalysis A: General, 2018, 568, 16-22. | 2.2 | 46 |
| 116 | Identification of Facetâ€Governing Reactivity in Hematite for Oxygen Evolution. Advanced Materials, 2018, 30, e1804341. | 11.1 | 96 |
| 117 | Spectroscopic Characterization and Mechanistic Studies on Visible Light Photoredox Carbon–Carbon Bond Formation by Bis(arylimino)acenaphthene Copper Photosensitizers. ACS Catalysis, 2018, 8, 11277-11286. | 5.5 | 42 |
| 118 | Ultra-high surface area graphitic Fe-N-C nanospheres with single-atom iron sites as highly efficient non-precious metal bifunctional catalysts towards oxygen redox reactions. Journal of Catalysis, 2018, 368, 279-290. | 3.1 | 105 |
| 119 | Metal–Oxygen Hybridization Determined Activity in Spinel-Based Oxygen Evolution Catalysts: A Case Study of ZnFe _{2–<i>x</i>} Cr _{<i>x</i>} O ₄ . Chemistry of Materials, 2018, 30, 6839-6848. | 3.2 | 65 |
| 120 | Necklace-like Multishelled Hollow Spinel Oxides with Oxygen Vacancies for Efficient Water Electrolysis. Journal of the American Chemical Society, 2018, 140, 13644-13653. | 6.6 | 430 |
| 121 | Hydrazone-based covalent organic frameworks for Lewis acid catalysis. Dalton Transactions, 2018, 47, 13824-13829. | 1.6 | 39 |
| 122 | Hybrid Nanomaterials with Single-Site Catalysts by Spatially Controllable Immobilization of Nickel Complexes <i>via</i> Photoclick Chemistry for Alkene Epoxidation. ACS Nano, 2018, 12, 5903-5912. | 7.3 | 16 |
| 123 | Lithiation-induced amorphization of Pd3P2S8 for highly efficient hydrogen evolution. Nature Catalysis, 2018, 1, 460-468. | 16.1 | 247 |
| 124 | Electronic and Defective Engineering of Electrospun CaMnO ₃ Nanotubes for Enhanced Oxygen Electrocatalysis in Rechargeable Zinc–Air Batteries. Advanced Energy Materials, 2018, 8, 1800612. | 10.2 | 234 |
| 125 | An electron deficiency strategy for enhancing hydrogen evolution on CoP nano-electrocatalysts. Nano Energy, 2018, 50, 273-280. | 8.2 | 89 |
| 126 | Identifying the Origin and Contribution of Surface Storage in TiO ₂ (B) Nanotube Electrode by In Situ Dynamic Valence State Monitoring. Advanced Materials, 2018, 30, e1802200. | 11.1 | 90 |

Уомдниа Du

| # | Article | IF | CITATIONS |
|-----|--|------|-----------|
| 127 | Host–Guest and Photophysical Behavior of Ti ₈ L ₁₂ Cube with Encapsulated [Ti(H ₂ O) ₆] Species. Chemistry - A European Journal, 2018, 24, 14358-14362. | 1.7 | 24 |
| 128 | Enlarged CoO Covalency in Octahedral Sites Leading to Highly Efficient Spinel Oxides for Oxygen Evolution Reaction. Advanced Materials, 2018, 30, e1802912. | 11.1 | 338 |
| 129 | Single-Atomic Cu with Multiple Oxygen Vacancies on Ceria for Electrocatalytic CO ₂ Reduction to CH ₄ . ACS Catalysis, 2018, 8, 7113-7119. | 5.5 | 486 |
| 130 | Engineering Sulfur Defects, Atomic Thickness, and Porous Structures into Cobalt Sulfide Nanosheets for Efficient Electrocatalytic Alkaline Hydrogen Evolution. ACS Catalysis, 2018, 8, 8077-8083. | 5.5 | 219 |
| 131 | Redox-targeted catalysis for vanadium redox-flow batteries. Nano Energy, 2018, 52, 292-299. | 8.2 | 43 |
| 132 | Immediate hydroxylation of arenes to phenols via V-containing all-silica ZSM-22 zeolite triggered non-radical mechanism. Nature Communications, 2018, 9, 2931. | 5.8 | 66 |
| 133 | Identifying Influential Parameters of Octahedrally Coordinated Cations in Spinel ZnMn _{<i>x</i>} Co _{2–<i>x</i>} O ₄ Oxides for the Oxidation Reaction. ACS Catalysis, 2018, 8, 8568-8577. | 5.5 | 68 |
| 134 | Atomic engineering of high-density isolated Co atoms on graphene with proximal-atom controlled reaction selectivity. Nature Communications, 2018, 9, 3197. | 5.8 | 146 |
| 135 | Preparation of 1T′-Phase ReS _{2<i>x</i>} Se _{2(1-<i>x</i>)} (<i>x</i> = 0–1) Nanodots for Highly Efficient Electrocatalytic Hydrogen Evolution Reaction. Journal of the American Chemical Society, 2018, 140, 8563-8568. | 6.6 | 104 |
| 136 | Degree of Geometric Tilting Determines the Activity of FeO ₆ Octahedra for Water Oxidation. Chemistry of Materials, 2018, 30, 4313-4320. | 3.2 | 54 |
| 137 | Crystal Phase and Architecture Engineering of Lotusâ€Thalamusâ€Shaped Ptâ€Ni Anisotropic Superstructures for Highly Efficient Electrochemical Hydrogen Evolution. Advanced Materials, 2018, 30, e1801741. | 11.1 | 163 |
| 138 | Intrinsic or Interface Clustering-Induced Ferromagnetism in Fe-Doped In ₂ O ₃ -Diluted Magnetic Semiconductors. ACS Applied Materials & Interfaces, 2018, 10, 22372-22380. | 4.0 | 23 |
| 139 | Electrochemical oxidation of C3 saturated alcohols on Co3O4 in alkaline. Electrochimica Acta, 2017, 228, 183-194. | 2.6 | 45 |
| 140 | Improved Reversibility of Fe ³⁺ /Fe ⁴⁺ Redox Couple in Sodium Super Ion Conductor Type Na ₃ Fe ₂ (PO ₄) ₃ for Sodiumâ€ion Batteries. Advanced Materials, 2017, 29, 1605694. | 11.1 | 169 |
| 141 | Origin of Magnetism in Hydrothermally Aged 2-Line Ferrihydrite Suspensions. Environmental Science & Technology, 2017, 51, 2643-2651. | 4.6 | 16 |
| 142 | On the synthesis and performance of hierarchical nanoporous TS-1 catalysts. Microporous and Mesoporous Materials, 2017, 244, 83-92. | 2.2 | 29 |
| 143 | Spatial imaging and speciation of Cu in rice (Oryza sativa L.) roots using synchrotron-based X-ray microfluorescence and X-ray absorption spectroscopy. Chemosphere, 2017, 175, 356-364. | 4.2 | 44 |
| 144 | Enhanced oxygen evolution reaction by Co-O-C bonds in rationally designed Co3O4/graphene nanocomposites. Nano Energy, 2017, 33, 445-452. | 8.2 | 131 |

| # | Article | IF | CITATIONS |
|-----|--|------|-----------|
| 145 | Activating and Optimizing Activity of CoS ₂ for Hydrogen Evolution Reaction through the Synergic Effect of N Dopants and S Vacancies. ACS Energy Letters, 2017, 2, 1022-1028. | 8.8 | 229 |
| 146 | Unleashing the Power and Energy of LiFePO ₄ -Based Redox Flow Lithium Battery with a Bifunctional Redox Mediator. Journal of the American Chemical Society, 2017, 139, 6286-6289. | 6.6 | 70 |
| 147 | <i>Al-BL</i> 1.0: a program for automatic on-line beamline optimization using the evolutionary algorithm. Journal of Synchrotron Radiation, 2017, 24, 367-373. | 1.0 | 2 |
| 148 | Unique PCoN Surface Bonding States Constructed on g ₃ N ₄ Nanosheets for Drastically Enhanced Photocatalytic Activity of H ₂ Evolution. Advanced Functional Materials, 2017, 27, 1604328. | 7.8 | 329 |
| 149 | Lanthanum oxycarbonate modified Cu/Al ₂ O ₃ catalysts for selective hydrogenolysis of glucose to propylene glycol: base site requirements. Catalysis Science and Technology, 2017, 7, 4680-4690. | 2.1 | 22 |
| 150 | Ex situ XAS investigation of effect of binders on electrochemical performance of Li ₂ Fe(SO ₄) ₂ cathode. Journal of Materials Chemistry A, 2017, 5, 19963-19971. | 5.2 | 4 |
| 151 | Directly synthesized V-containing BEA zeolite: Acid-oxidation bifunctional catalyst enhancing C-alkylation selectivity in liquid-phase methylation of phenol. Chemical Engineering Journal, 2017, 328, 1031-1042. | 6.6 | 25 |
| 152 | Phosphonate-Based Metal–Organic Framework Derived Co–P–C Hybrid as an Efficient Electrocatalyst for Oxygen Evolution Reaction. ACS Catalysis, 2017, 7, 6000-6007. | 5.5 | 149 |
| 153 | Tailoring the Co 3d-O 2p Covalency in LaCoO ₃ by Fe Substitution To Promote Oxygen Evolution Reaction. Chemistry of Materials, 2017, 29, 10534-10541. | 3.2 | 254 |
| 154 | Encapsulating porous SnO ₂ into a hybrid nanocarbon matrix for long lifetime Li storage. Journal of Materials Chemistry A, 2017, 5, 25609-25617. | 5.2 | 57 |
| 155 | Selective conversion of lactic acid to acrylic acid over alkali and alkaline-earth metal co-modified NaY zeolites. Catalysis Science and Technology, 2017, 7, 6101-6111. | 2.1 | 26 |
| 156 | The role of metal–support interaction for CO-free hydrogen from low temperature ethanol steam reforming on Rh–Fe catalysts. Physical Chemistry Chemical Physics, 2017, 19, 4199-4207. | 1.3 | 25 |
| 157 | Confocal depth-resolved fluorescence micro-X-ray absorption spectroscopy for the study of cultural heritage materials: a new mobile endstation at the Beijing Synchrotron Radiation Facility. Journal of Synchrotron Radiation, 2017, 24, 1000-1005. | 1.0 | 11 |
| 158 | Anion vacancy-mediated ferromagnetism in atomic-thick Ni3N nanosheets. Applied Physics Letters, 2017, 111, . | 1.5 | 11 |
| 159 | Nitrogen-doped cobalt phosphate@nanocarbon hybrids for efficient electrocatalytic oxygen reduction. Energy and Environmental Science, 2016, 9, 2563-2570. | 15.6 | 216 |
| 160 | Unravelling the anomalous electrical and optical phase-change characteristics in FeTe. Acta Materialia, 2016, 112, 67-76. | 3.8 | 16 |
| 161 | Intrinsically Conductive Perovskite Oxides with Enhanced Stability and Electrocatalytic Activity for Oxygen Reduction Reactions. ACS Catalysis, 2016, 6, 7865-7871. | 5.5 | 51 |
| 162 | One-Pot Synthesis of Fe(III)–Polydopamine Complex Nanospheres: Morphological Evolution, Mechanism, and Application of the Carbonized Hybrid Nanospheres in Catalysis and Zn–Air Battery. Langmuir, 2016, 32, 9265-9275. | 1.6 | 78 |

| # | Article | IF | CITATIONS |
|-----|--|-------------------------|-----------|
| 163 | Intrinsic Ferromagnetism in the Diluted Magnetic Semiconductor <mml:math xmlns:mml="http://www.w3.org/1998/Math/MathML" display="inline"><mml:mrow><mml:mi>Co</mml:mi><mml:mo>:</mml:mo><mml:msub><mml:mrow><mml:mi> Physical Review Letters, 2016, 117, 227202.</mml:mi></mml:mrow></mml:msub></mml:mrow></mml:math | Ti <mark>O</mark> ?/mml | ::mi> |
| 164 | Oxygen Tuned Local Structure and Phase-Change Performance of Germanium Telluride. ACS Applied Materials & amp; Interfaces, 2016, 8, 20185-20191. | 4.0 | 40 |
| 165 | One-pot synthesis of polydopamine–Zn complex antifouling coatings on membranes for ultrafiltration under harsh conditions. RSC Advances, 2016, 6, 103390-103398. | 1.7 | 26 |
| 166 | Polyoxometalate immobilized in MIL-101(Cr) as an efficient catalyst for water oxidation. Applied Catalysis A: General, 2016, 521, 83-89. | 2.2 | 70 |
| 167 | High-performance NaFePO ₄ formed by aqueous ion-exchange and its mechanism for advanced sodium ion batteries. Journal of Materials Chemistry A, 2016, 4, 4882-4892. | 5.2 | 129 |
| 168 | <i>In Situ</i> Raman Spectroscopy of Copper and Copper Oxide Surfaces during Electrochemical Oxygen Evolution Reaction: Identification of Cu ^{III} Oxides as Catalytically Active Species. ACS Catalysis, 2016, 6, 2473-2481. | 5.5 | 592 |
| 169 | Highly efficient rutile TiO ₂ photocatalysts with single Cu(<scp>ii</scp>) and Fe(<scp>iii</scp>) surface catalytic sites. Journal of Materials Chemistry A, 2016, 4, 3127-3138. | 5.2 | 73 |
| 170 | A Stepâ€byâ€Step Assembly of a 3D Coordination Polymer in the Solidâ€State by Desolvation and [2+2] Cycloaddition Reactions. Chemistry - A European Journal, 2015, 21, 11948-11953. | 1.7 | 26 |
| 171 | Frontispiece: A Step-by-Step Assembly of a 3D Coordination Polymer in the Solid-State by Desolvation and [2+2] Cycloaddition Reactions. Chemistry - A European Journal, 2015, 21, n/a-n/a. | 1.7 | 0 |
| 172 | High-temperature water–gas shift reaction over Ni/xK/CeO2 catalysts: Suppression of methanation via formation of bridging carbonyls. Journal of Catalysis, 2015, 329, 130-143. | 3.1 | 87 |
| 173 | Bifunctional Mo3VOx/H4SiW12O40/Al2O3 catalysts for one-step conversion of glycerol to acrylic acid: Catalyst structural evolution and reaction pathways. Applied Catalysis B: Environmental, 2015, 174-175, 1-12. | 10.8 | 17 |
| 174 | Facile synthesis of copper nanoparticles in glycerol at room temperature: formation mechanism. RSC Advances, 2015, 5, 24544-24549. | 1.7 | 40 |
| 175 | β-FeOOH: An Earth-Abundant High-Capacity Negative Electrode Material for Sodium-Ion Batteries. Chemistry of Materials, 2015, 27, 5340-5348. | 3.2 | 57 |
| 176 | XAFCA: a new XAFS beamline for catalysis research. Journal of Synchrotron Radiation, 2015, 22, 839-843. | 1.0 | 125 |
| 177 | General method for automatic on-line beamline optimization based on genetic algorithm. Journal of Synchrotron Radiation, 2015, 22, 661-665. | 1.0 | 5 |
| 178 | Highly dispersed supported metal catalysts prepared via in-situ self-assembled core-shell precursor route. International Journal of Hydrogen Energy, 2015, 40, 13388-13398. | 3.8 | 19 |
| 179 | Metal–organic framework immobilized cobalt oxide nanoparticles for efficient photocatalytic water oxidation. Journal of Materials Chemistry A, 2015, 3, 20607-20613. | 5.2 | 57 |
| 180 | Fe2O3 Nanoparticle/SWCNT Composite Electrode for Sensitive Electrocatalytic Oxidation of Hydroquinone. Electrochimica Acta, 2015, 180, 1059-1067. | 2.6 | 43 |

| # | Article | IF | CITATIONS |
|-----|--|--------------------------|-----------|
| 181 | Superior Lithium Storage Properties of βâ€FeOOH. Advanced Energy Materials, 2015, 5, 1401517. | 10.2 | 56 |
| 182 | Supported H4SiW12O40/Al2O3 solid acid catalysts for dehydration of glycerol to acrolein: Evolution of catalyst structure and performance with calcination temperature. Applied Catalysis A: General, 2015, 489, 32-41. | 2.2 | 56 |
| 183 | Bimetallic Ni–Cu catalyst supported on CeO2 for high-temperature water–gas shift reaction: Methane suppression via enhanced CO adsorption. Journal of Catalysis, 2014, 314, 32-46. | 3.1 | 268 |
| 184 | Disruption of Putrescine Biosynthesis in Shewanella oneidensis Enhances Biofilm Cohesiveness and Performance in Cr(VI) Immobilization. Applied and Environmental Microbiology, 2014, 80, 1498-1506. | 1.4 | 101 |
| 185 | Incorporation of Cl into sequentially deposited lead halide perovskite films for highly efficient mesoporous solar cells. Nanoscale, 2014, 6, 13854-13860. | 2.8 | 76 |
| 186 | Speciation and localization of Zn in the hyperaccumulator Sedum alfredii by extended X-ray absorption fine structure and micro-X-ray fluorescence. Plant Physiology and Biochemistry, 2014, 84, 224-232. | 2.8 | 30 |
| 187 | Rh–Fe/Ca–Al2O3: A Unique Catalyst for CO-Free Hydrogen Production in Low Temperature Ethanol Steam Reforming. Topics in Catalysis, 2014, 57, 627-636. | 1.3 | 10 |
| 188 | Data analysis method to achieve sub-10â€pm spatialÂresolution using extended X-ray absorption fine-structure spectroscopy. Journal of Synchrotron Radiation, 2014, 21, 756-761. | 1.0 | 11 |
| 189 | Post-synthesis modification of a metal–organic framework to construct a bifunctional photocatalyst for hydrogen production. Energy and Environmental Science, 2013, 6, 3229. | 15.6 | 336 |
| 190 | The structure of Mn-doped tris(8-hydroxyquinoline)gallium by extended x-ray absorption fine structure spectroscopy and first principles calculations. Journal of Applied Physics, 2012, 112, 113519. | 1.1 | 5 |
| 191 | Thickness-dependent twinning evolution and ferroelectric behavior of epitaxial <mml:math xmlns:mml="http://www.w3.org/1998/Math/MathML" display="inline"><mml:mrow><mml:msub><mml:mrow><mml:mtext>BiFeO</mml:mtext></mml:mrow><mml:m thin films. Physical Review B. 2010. 82</mml:m </mml:msub></mml:mrow></mml:math | n> ¹ 1 /mm | l:mn> |
| 192 | Spatial Imaging and Speciation of Lead in the Accumulator Plant <i>Sedum alfredii</i> by Microscopically Focused Synchrotron X-ray Investigation. Environmental Science & amp; Technology, 2010, 44, 5920-5926. | 4.6 | 89 |
| 193 | A new cell for X-ray absorption spectroscopy study under high pressure. Chinese Physics C, 2009, 33, 701-705. | 1.5 | 3 |
| 194 | Projected gradient methods for synchrotron radiation spectra distribution function reconstruction. Inverse Problems in Science and Engineering, 2009, 17, 175-186. | 1.2 | 2 |
| 195 | Mechanism of removal of arsenic by bead cellulose loaded with iron oxyhydroxide (β-FeOOH): EXAFS study. Journal of Colloid and Interface Science, 2007, 314, 427-433. | 5.0 | 86 |
| 196 | On projected gradient methods for regularizing reconstruction of synchrotron radiation spectra distribution function. Proceedings in Applied Mathematics and Mechanics, 2007, 7, 1061901-1061902. | 0.2 | 0 |
| 197 | Measurement of synchrotron radiation spectra using combined attenuation method and regularized inversion. Nuclear Instruments and Methods in Physics Research, Section A: Accelerators, Spectrometers, Detectors and Associated Equipment, 2006, 565, 855-860. | 0.7 | 8 |